Image frequency suppression in frequency-scanned direction-of-arrival estimation systems

W. Wasylkiwskyj, I. Kopriva and M. Doroslovački

Abstract: A novel signal processing approach to the problem of image frequency suppression in wide-band frequency-scanned radio frequency (RF) receiving arrays that employ digital signal processing (DSP) techniques to estimate the direction of arrival (DOA) of incoming radiation has been presented. The conventional approach to image rejection in RF receivers is to employ a front-end RF tuner before downconversion to the intermediate frequency. As DOA processing employs a separate receiver channel for each array element, an RF tuner would be needed behind each element. Clearly for scanned systems at microwave frequencies, this is not a viable option where the tuners would generally have to be implemented in RF hardware. The need for RF tuners can be eliminated by downconversion down to baseband and employing I&Q mixers, which provide an intrinsic image rejection capability. Unfortunately, such a solution requires two analog-to-digital (A/D) converters per array element. An alternative approach is to use image rejection mixers in which case only one A/D converter per array element is needed. The approach also requires only one A/D per array element but achieves the image rejection through a DSP implementation. As a result, use of relatively expensive image rejection mixers is avoided without sacrificing performance. Experimental results are presented that validate the theoretical predictions.

1 Introduction

Typical DF algorithms, such as MUSIC [1] or Root-MUSIC [2, 3], employ the sample covariance matrix estimated from digital data to determine the direction of arrival (DOA) of signals incident on the array. Usually, the frequency content of the incident signals is too high for direct analog-to-digital (A/D) conversion so that some form of frequency downconversion is necessary before the array outputs can be transformed into digital data streams. An important practical issue in designing a frequency-scanned DOA system is the rejection of contributions in the image frequency bands. The conventional approach to image rejection in radio frequency (RF) receivers is to employ a front-end RF tuner before downconversion to the intermediate frequency (IF). As DOA processing employs a separate receiver channel for each array element, one would need an RF tuner behind each element. For scanned systems at microwave frequencies, this is not a viable option where the tuners would generally have to be implemented at RF in hardware. An alternative approach is to exploit the intrinsic image rejection capability of an I&Q mixer using such a mixer at the output of each array element. This is achieved by splitting the RF output of each array element into two parallel channels and using individual local oscillator (LO) inputs in phase quadrature to drive each of the two mixer cells. Fixed low-pass anti-aliasing filters in each of the two (I and Q) channels can then be used to set the required sampling rate and provide the necessary frequency selectivity, whereas tuning over the RF band can be effected by changing the LO frequency. Evidently, this scheme requires two A/D converters per array element, which (particularly in case of high-speed converters) are high-cost items in DOA implementations.

Clearly, the number of required A/D converters can be cut in half using only a single-channel mixer (one mixer cell) per array element and recovering the required I&Q channel data in software (e.g. using Hilbert transforms). This can be done provided a suitable technique is employed to remove the contribution from the image frequency band. Conceptually, the simplest approach is to employ an RF bandpass filter at the output of each array element. This is particularly cumbersome and expensive if the LO must be tuned over a band of frequencies, and then the image rejection filter must be tunable as well. Alternatively, by employing a sufficiently high and fixed IF to cover the desired tuning band (and for a large tuning bandwidth requiring a high-speed A/D converter), a fixed RF stop band filter (or a bandpass filter centred at the desired band) can be employed to remove image contributions. All subsequent filtering (whether fixed or variable) as well as the I&Q channel formation can then be done in software. An obvious drawback of this scheme is that for large tuning ranges, the required speed of the A/D converter may become impractically high.

Yet another way of avoiding the need for more than one A/D converter per array element is to use image rejection mixers. Similar to the dual-channel downconverter, such a mixer employs two LO inputs having 90° relative phase shift, resulting in two channels each modulated by a carrier at the (non-zero) difference frequency. After filtering both channels and phase shifting one of them by 90°, subtraction (or addition) of the two outputs can be made to yield the desired lower (upper) sideband. This purely analogue operation can then be followed by an A/D and I&Q channel reconstruction implemented digitally. From the standpoint of DOA estimation, this approach suffers from

doi:10.1049/iet-rsn:20050078
Paper first received 22nd July 2005 and in revised form 6th February 2007
The authors are with Department of Electrical and Computer Engineering, The George Washington University, 801 22nd St., NW, Washington, DC 20052, USA
E-mail: ikopriva@gmail.com

two drawbacks. One is that compared with a single mixer cell unit, an image rejection mixer is quite expensive. The other is that image rejection of 25 dB or better required in high-quality DOA estimation systems is difficult to achieve consistently, particularly over wide bandwidths.

This paper presents an approach that employs a single-channel mixer per array element and removes the contribution from the image frequency bands through recursive subtraction of the array sample covariance matrix. Although not suitable for demodulation of information-bearing signals, this technique affords a cost-effective way of implementing DOA algorithms that rely on estimates of second-order statistics of incoming radiation.

2 DOA problem formulation

The problem of estimating the DOA of L uncorrelated plane waves incident on an N-element array is formulated in terms of the complex low-pass equivalents of the RF signals as [4]

$$\boldsymbol{z}(t) = \boldsymbol{A}\boldsymbol{s}(t) + \boldsymbol{v}(t) \tag{1}$$

where $\boldsymbol{z}(t)$ is an N-dimensional column vector representing the array outputs, $\boldsymbol{A}$ is the $N'L$ array steering matrix, $\boldsymbol{s}(t)$ is an L-dimensional column vector representing the L signals incident on the array, whereas the column vector $\boldsymbol{n}(t)$ (comprised mutually uncorrelated elements entries) represents receiver noise. Moreover, the noise powers s^2 are assumed all identical, that is,

$$\langle \boldsymbol{v}(t)\boldsymbol{v}^H(t)\rangle = s^2\boldsymbol{I}_N \; \langle \boldsymbol{v}(t)\boldsymbol{v}^H(t)\rangle = \sigma^2\boldsymbol{I}_N$$

where á ñ denotes ensemble average and $\boldsymbol{I}_N$ is the $N'N$ identity matrix. For a linear array of uniformly spaced vertical electric dipoles, the elements of the steering matrix are given by

$$a_{nl} = a_n(\theta_l, \varphi_l) = -\frac{\mathrm{j}\lambda}{\sqrt{\zeta_0}}\hat{f}_n(\theta_l, \varphi_l) \times \exp(\mathrm{j}nk_0 d \sin\theta_l \cos\varphi_l), \quad n = 1, 2, \ldots, N, \quad l = 1, 2, \ldots, L \tag{2}$$

where θ_l, φ_l are spherical polar coordinates specifying the direction of incidence of the signal from the lth emitter, $k_0 = 2\pi/\lambda$ is a free space wavenumber evaluated at the nominal carrier frequency, d is the inter-element spacing, z_0 is the characteristic impedance of free space and $\hat{f}_n(\theta_l, \varphi_l)$ is the component of the radiation (electric) field of the nth array element along the electric field of the linearly polarised plane wave incident from the lth direction. It is worth noting that the elementary radiation pattern $\hat{f}_n(\theta, \varphi)$ is not that of an array element in isolation, but is to be measured when all other elements are terminated in suitably defined dissipative loads [5, 6]. Thus $\hat{f}_n(\theta, \varphi)$ depends implicitly on the mutual interaction among the array elements. The approximation

$$\hat{f}_n(\theta, \varphi) \simeq \text{constant} \times \hat{f}(\theta, \varphi) \tag{3}$$

(so that the element patterns are independent of the antenna index n) frequently employed in theoretical developments of DOA algorithms is generally not well satisfied by real physical elements. Notable exceptions are long linear arrays of identical elements wherein most of the interior elements can be made to experience the environment of an infinite linear array (which condition can be approximated with a relatively small finite array by appending extra terminated 'dummy' elements at the array edges [7]) and linear arrays whose outputs have been modified by a decoupling transform. Under these circumstances, the computational complexity of DOA algorithms can be substantially reduced by resorting to root-based DF algorithms [2, 3].

Both search-based DF algorithm, such as MUSIC, or root-based DF algorithms, such as root-MUSIC or modified root polynomial (MRP) [8], employ the eigen-decomposition of the array data sample covariance matrix calculated from the complex baseband outputs as

$$\boldsymbol{R} = \overline{\boldsymbol{z}\boldsymbol{z}^H} = \boldsymbol{A}\overline{\boldsymbol{s}\boldsymbol{s}^H}\boldsymbol{A}^H + \overline{\boldsymbol{v}\boldsymbol{v}^H} \tag{4}$$

where the overbar denotes temporal averaging. For the sample covariance matrix, this temporal average reads

$$r_{ij} = \frac{1}{T}\sum_{t=1}^{T} z_i(t)z_j^*(t), \quad 1 \le i, j \le N \tag{5}$$

where T is the sample size and r_{ij} is an element of $\boldsymbol{R}$.

3 Image suppression technique

We consider an N-element linear array of uniformly spaced elements with L incident signals spanning the bandwidth w_W rps. For processing purposes, this bandwidth is divided into M non-overlapping frequency bins each of width Dw rps shown in Fig. 1. A typical signal whose energy is confined to such a frequency bin has the bandpass representation

$$s_{lp}^{(\mathrm{BP})}(t) = x_{lp}(t)\cos\omega_p t - y_{lp}(t)\sin\omega_p t \tag{6}$$

where w_p is the nominal carrier frequency [as neither the modulation nor the true carrier frequency of the incident signals are known, the 'carrier frequency' w_p is merely an assigned number that corresponds to the band centre of

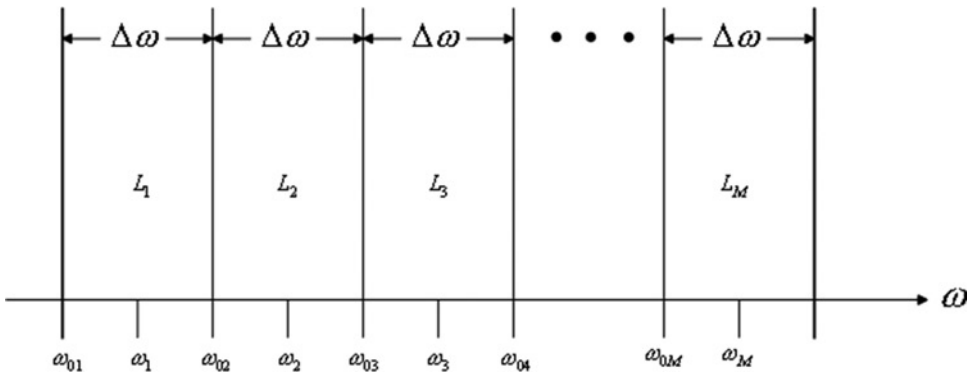

Fig. 1 *Relative positions of LO and bin centre frequencies for a scanned DOA system*

frequency bin p in Fig. 1] at the M band centres in Fig. 1 and $x_{lp}(t)$ and $y_{lp}(t)$ are real and imaginary parts, respectively, of the complex low-pass signal

$$s_{lp}(t) = x_{lp}(t) + \mathrm{j}y_{lp}(t) \tag{7}$$

It is supposed that the pth frequency bin contains L_p incident signals. Hence

$$L = \sum_{p=1}^{M} L_p \tag{8}$$

with $L_p < N, p = 1, 2, \ldots, M$. On the basis of (1) and (2) and assuming a sufficiently small array so that Dw is compatible with the narrow band model, the RF response of the nth array element may be represented by

$$b_n(t) = \mathrm{Re}\left\{ \sum_{p=1}^{M} \sum_{l \in L_p} \left[-\frac{\mathrm{j}\lambda_p}{\sqrt{\zeta_0}} \hat{f}_n(\Omega_{lp}, \omega_p) \right] \times \mathrm{e}^{\mathrm{j}n\omega_p d \cos \psi_{lp}/c} s_{lp}(t)\, \mathrm{e}^{\mathrm{j}\omega_p t} \right\} \tag{9}$$

where W_{lp} denotes the spherical coordinate pair of the direction of incidence of the lth signal within frequency bin p, c is the speed of light in vacuo, y_{lp} is the angle between the incidence direction and the array axis ($\cos \psi_{lp} = \sin \theta_{lp} \cos \varphi_{lp}$) and l_p is the wavelength at the nominal carrier frequency w_p. (The normalisation of the element patterns adopted herein is such that $\int_{-\infty}^{\infty} b_n^2(t)\, \mathrm{d}t$ represents the total energy absorbed by the Thevenin equivalent load connected to the nth array element.). For notational compactness, set

$$\frac{-\mathrm{j}\lambda_p}{\sqrt{\zeta_0}} \hat{f}_n(\Omega_{lp}, \omega_p) = \frac{\lambda_p}{\sqrt{\zeta_0}} |\hat{f}_n(\Omega_{lp}, \omega_p)| \mathrm{e}^{\mathrm{j}\Psi_n(\psi_{lp}, \omega_p)} = A_n(\Omega_{lp}, \omega_p) \mathrm{e}^{j\Psi_n(\psi_{lp}, \omega_p)} \tag{10}$$

Furthermore, let

$$\bar{\theta}_{nlp} = \frac{n\omega_p d \cos \psi_{lp}}{c} + \Psi_n(\psi_{lp}, \omega_p) \tag{11}$$

so that (9) can be rewritten as

$$b_n(t) = \sum_{p=1}^{M} b_{np}(t) = \sum_{p=1}^{M} \sum_{l \in L_p} A_n(\Omega_{lp}, \omega_p) \times [x'_{lpn}(t) \cos \omega_p t - y'_{lpn}(t) \sin \omega_p t] \tag{12}$$

where

$$x'_{lpn}(t) = x_{lp}(t) \cos \bar{\theta}_{nlp} - y_{lp}(t) \sin \bar{\theta}_{nlp},$$
$$y'_{lpn}(t) = x_{lp}(t) \sin \bar{\theta}_{nlp} + y_{lp}(t) \cos \bar{\theta}_{nlp}$$

Each of the array outputs is fed to its mixer cell with LO frequencies w_{0q} set sequentially to

$$\omega_{0q} = \omega_q - \frac{\Delta\omega}{2}, \quad q = 1, 2, 3, \ldots, M \tag{13}$$

as indicated in Fig. 1. The product of the LO input to mixer n, $\cos(\omega_{0q} t + \delta_n)$, where d_n represents phase offset, and the signal $b_n(t)$ in (12) gives (omitting the sum frequency terms as they will be filtered)

$$b_{nq}^{(\mathrm{IF})}(t) = \frac{1}{2} \sum_{p=1}^{M} \sum_{l \in L_p} A_n(\Omega_{lp}, \omega_p) \times \left\{ x''_{lpn}(t) \cos\left[\left(\omega_p - \omega_q + \frac{\Delta\omega}{2} \right) t \right] - y''_{lpn}(t) \sin\left[\left(\omega_p - \omega_q + \frac{\Delta\omega}{2} \right) t \right] \right\} \tag{14}$$

where

$$x''_{lpn}(t) = x_{lp}(t) \cos(\bar{\theta}_{nlp} - \delta_n) - y_{lp}(t) \sin(\bar{\theta}_{nlp} - \delta_n),$$
$$y''_{lpn}(t) = x_{lp}(t) \sin(\bar{\theta}_{nlp} - \delta_n) + y_{lp}(t) \cos(\bar{\theta}_{nlp} - \delta_n) \tag{15}$$

Evaluating (14) for $q = 1$ results in

$$b_{n1}^{(\mathrm{IF})}(t) = \frac{1}{2} \sum_{l \in L_1} A_n(\Omega_{l1}, \omega_1) \times \left[x''_{l1n}(t) \cos\left(\frac{\Delta\omega t}{2} \right) - y''_{l1n}(t) \sin\left(\frac{\Delta\omega t}{2} \right) \right] + \frac{1}{2} \sum_{p=2}^{M} \sum_{l \in L_p} A_n(\Omega_{l1}, \omega_p) \times \left\{ x''_{lpn}(t) \cos\left[\left(p - \frac{1}{2} \right) \Delta\omega t \right] - y''_{lpn}(t) \sin\left[\left(p - \frac{1}{2} \right) \Delta\omega t \right] \right\} \tag{16}$$

By construction, the spectra of the signal components $x''_{l1n}(t)$ and $y''_{l1n}(t)$ entering into the first sum in (16) are limited to $|\omega| < \Delta\omega/2$, so that the modulation by sinusoids of frequency $\Delta w/2$ increases the spectral occupancy to at most $|\omega| < \Delta\omega$. Modulation of signal components entering into second sum will shift the spectra outside this range. Consequently, a (ideal) low-pass filter with cutoff frequency $\omega = \Delta\omega$ will eliminate the second sum resulting in the output

$$\bar{b}_{n1}^{(\mathrm{IF})}(t) = \mathrm{Re}\left\{ \frac{1}{2} \sum_{l \in L_1} A_n(\Omega_{l1}, \omega_1) [x''_{l1n}(t) + \mathrm{j}y''_{l1n}(t)] \mathrm{e}^{\mathrm{j}\Delta\omega t/2} \right\} \tag{17}$$

Because $x''_{l1n}(t) + \mathrm{j}y''_{l1n}(t)$ are assumed band-limited to $|\omega| < \Delta\omega/2$, the signal defined by the sum in braces is analytic. It can be recovered from $\bar{b}_{n1}^{(\mathrm{IF})}(t)$ with the aid of Hilbert transform. Thus

$$H\{\bar{b}_{n1}^{(\mathrm{IF})}(t)\} = \frac{1}{2} \sum_{l \in L_1} A_n(\Omega_{l1}, \omega_1) \times \left[x''_{l1n}(t) \sin\left(\frac{\Delta\omega t}{2} \right) + y''_{l1n}(t) \cos\left(\frac{\Delta\omega t}{2} \right) \right] \tag{18}$$

and one obtains

$$z_{n1}(t) = \left[\bar{b}_{n1}^{(\mathrm{IF})}(t) + \mathrm{j}H\left\{ \bar{b}_{n1}^{(\mathrm{IF})}(t) \right\} \right] \mathrm{e}^{-\Delta\omega t/2} = \frac{1}{2} \sum_{l \in L_1} A_n(\Omega_{l1}, \omega_1) [x''_{l1n}(t) + \mathrm{j}y''_{l1n}(t)] = \frac{-\mathrm{j}\lambda_1}{\sqrt{\zeta_0}} \sum_{l \in L_1} \hat{f}_n(\Omega_{l1}, \omega_1) \mathrm{e}^{\mathrm{j}(n\omega_1 d \cos \psi_{l1}/c - \delta_n)} s_{l1}(t) \tag{19}$$

which is identical to (12) for $q = 1$. Evidently, this result assumes that there are no signals with frequencies lower than $\omega_1 - \Delta\omega/2$ which can always be enforced by a fixed RF high-pass filter. Proceeding to $q = 2$ in (14) gives

$$\begin{aligned} b_{n2}^{(\mathrm{IF})}(t) = & \frac{1}{2}\sum_{l\in L_1} A_n(\Omega_{l1}, \omega_1) \\ & \times \left[x''_{l1n}(t)\cos\left(\frac{\Delta\omega t}{2}\right) + y''_{l1n}(t)\sin\left(\frac{\Delta\omega t}{2}\right)\right] \\ & + \frac{1}{2}\sum_{l\in L_2} A_n(\Omega_{l2}, \omega_2) \\ & \times \left[x''_{l2n}(t)\cos\left(\frac{\Delta\omega t}{2}\right) - y''_{l2n}(t)\sin\left(\frac{\Delta\omega t}{2}\right)\right] \\ & + \frac{1}{2}\sum_{p=3}^{M}\sum_{l\in L_p} A_n(\Omega_{lp}, \omega_p) \\ & \times \left\{x''_{lpn}(t)\cos\left[\left(p-\frac{3}{2}\right)\Delta\omega t\right] \right. \\ & \left. - y''_{lpn}(t)\sin\left[\left(p-\frac{3}{2}\right)\Delta\omega t\right]\right\} \end{aligned} \tag{20}$$

Again a low-pass filter with cutoff at $w = \Delta w$ will reject the last sum of (20) and the output of the A/D converter will be

$$\begin{aligned} \bar{b}_{n2}^{(\mathrm{IF})}(t) = & \frac{1}{2}\sum_{l\in L_1} A_n(\Omega_{l1}, \omega_1) \\ & \times \left[x''_{l1n}(t)\cos\left(\frac{\Delta\omega t}{2}\right) + y''_{l1n}(t)\sin\left(\frac{\Delta\omega t}{2}\right)\right] \\ & + \frac{1}{2}\sum_{l\in L_2} A_n(\Omega_{l2}, \omega_2) \\ & \times \left[x''_{l2n}(t)\cos\left(\frac{\Delta\omega t}{2}\right) - y''_{l2n}(t)\sin\left(\frac{\Delta\omega t}{2}\right)\right] \end{aligned} \tag{21}$$

which can be written in the alternative form

$$\begin{aligned} \bar{b}_{n2}^{(\mathrm{IF})}(t) = \mathrm{Re}\Bigg\{ & \frac{1}{2}\sum_{l\in L_1} A_n(\Omega_{l1}, \omega_1) \\ & \times \left[x''_{l1n}(t)\cos\left(\frac{\Delta\omega t}{2}\right) + y''_{l1n}(t)\sin\left(\frac{\Delta\omega t}{2}\right)\right] \\ & \times \mathrm{e}^{\mathrm{j}\Delta\omega t/2} + \frac{1}{2}\sum_{l\in L_2} A_n(\Omega_{l2}, \omega_2) \\ & \times \left[x''_{l2n}(t)\cos\left(\frac{\Delta\omega t}{2}\right) \right. \\ & \left. - y''_{l2n}(t)\sin\left(\frac{\Delta\omega t}{2}\right)\right] e^{\mathrm{j}\Delta\omega t/2}\Bigg\} \end{aligned} \tag{22}$$

The quantity in braces is a sum of two analytic signals the first of which corresponds to the image frequency band $\omega_1 - \Delta\omega/2 < \omega < \omega_1 + \Delta\omega/2$ and the second to the selected band $\omega_2 - \Delta\omega/2 < \omega < \omega_2 + \Delta\omega/2$. Following the same procedure as in (17), the output analytic signal is reconstructed from A/D converter data corresponding to the nth array element as

$$\begin{aligned} z_{n2}(t) &= \left[\bar{b}_{n2}^{(\mathrm{IF})}(t) + \mathrm{j}H\left\{\bar{b}_{n2}^{(\mathrm{IF})}(t)\right\}\right]\mathrm{e}^{-\Delta\omega t/2} \\ &= \frac{\mathrm{j}\lambda_1}{\sqrt{\zeta_0}}\sum_{l\in L_1}\hat{f}_n^*(\Omega_{l1}, \omega_1)\mathrm{e}^{-\mathrm{j}(n\omega_1 d\cos\psi_{l1}/c - \delta_n)}s_{l1}^*(t) \\ &\quad + \frac{-j\lambda_1}{\sqrt{\zeta_0}}\sum_{l\in L_2}\hat{f}_n(\Omega_{l2}, \omega_2)\mathrm{e}^{j(n\omega_2 d\cos\psi_{l2}/c - \delta_n)}s_{l2}(t) \end{aligned} \tag{23}$$

and, in general, for each of the M bands, $q = 1, 2, 3, \ldots, M$.

$$\begin{aligned} z_{nq}(t) = & \left[\bar{b}_{nq}^{(\mathrm{IF})}(t) + \mathrm{j}H\left\{\bar{b}_{nq}^{(\mathrm{IF})}(t)\right\}\right]\mathrm{e}^{-\Delta\omega t/2} \\ = & \frac{\mathrm{j}\lambda_{q-1}}{\sqrt{\zeta_0}}\sum_{l\in L_{q-1}} \\ & \times \hat{f}_n^*(\Omega_{lq-1}, \omega_{q-1})\mathrm{e}^{-\mathrm{j}(n\omega_{q-1}d\cos\psi_{lq-1}/c - \delta_n)}s_{lq-1}^*(t) \\ & + \frac{-\mathrm{j}\lambda_q}{\sqrt{\zeta_0}}\sum_{l\in L_q}\hat{f}_n(\Omega_{lq}, \omega_q)\mathrm{e}^{\mathrm{j}(n\omega_q d\cos\psi_{lq}/c - \delta_n)}s_{lq}(t) \end{aligned} \tag{24}$$

Assuming that RF high-pass filter blocks the reception for $\omega < \omega_1 - \Delta\omega/2 = \omega_{01}$, the sequence may be initialised with $s_{l0}(t) = 0$. Rewriting now (24) in the matrix notation of (1) and (2) and redefining $z_{nq}(t)$ by the receiver noise term yields

$$\boldsymbol{z}_q(t) = \boldsymbol{A}_q\boldsymbol{s}_q(t) + \boldsymbol{A}_{q-1}^*\boldsymbol{s}_{q-1}^*(t) + \boldsymbol{\nu}(t) \tag{25}$$

We assume that M data sequences are of equal duration and long enough to accurately estimate data covariance matrices. Then if the signals $\boldsymbol{s}_q(t)$ and $\boldsymbol{s}_{q-1}(t)$ are mutually uncorrelated, one obtains from (25)

$$\overline{\boldsymbol{z}_q\boldsymbol{z}_q^H} = \boldsymbol{A}_q\overline{\boldsymbol{s}_q\boldsymbol{s}_q^H}\boldsymbol{A}_q^H + \boldsymbol{A}_{q-1}^*\overline{\boldsymbol{s}_{q-1}^*\boldsymbol{s}_{q-1}^T}\boldsymbol{A}_{q-1}^T + \overline{\boldsymbol{\nu}\boldsymbol{\nu}^H} \tag{26}$$

where array covariance matrix is estimated for the zero lag on the time window of length T in accordance with

$$\overline{\boldsymbol{z}_q(t)\boldsymbol{z}_q^H(t)} = \frac{1}{T}\sum_{t=(q-1)T}^{qT}\boldsymbol{z}_q(t)\boldsymbol{z}_q^H(t) \tag{27}$$

If we can assume that statistical nature of the signals and noise corresponding to (time) adjacent data records is substantially the same, (26) provides a recursive relation for computing the zarray covariance matrix of signals within each frequency bin. The covariance by definition is the quantity

$$\boldsymbol{R}_q = \boldsymbol{A}_q\overline{\boldsymbol{s}_q\boldsymbol{s}_q^H}\boldsymbol{A}_q^H + \overline{\boldsymbol{\nu}\boldsymbol{\nu}^H} \tag{28}$$

For a sufficiently long time record, $\overline{\boldsymbol{\nu}\boldsymbol{\nu}^H}$ approaches $\sigma^2\boldsymbol{I}_N$, which is a real diagonal matrix. Using this in (26), the recursion formula reads [note that for even q, the noise contribution cancels]

$$\boldsymbol{R}_q = \overline{\boldsymbol{z}_q\boldsymbol{z}_q^H} - \boldsymbol{R}_{q-1}^* \tag{29}$$

with initialisation $\boldsymbol{R}_0 = 0$.

A functional block diagram of the proposed image suppression technique for a representative array element is shown in Fig. 2 that includes the principal RF components, the A/D converter and the processing steps that yield z_{nq}. An actual hardware implementation may include additional components (e.g. RF and IF amplifiers). An important practical issue in the implementation is the inevitable imperfection of the RF components that will tend to limit the degree

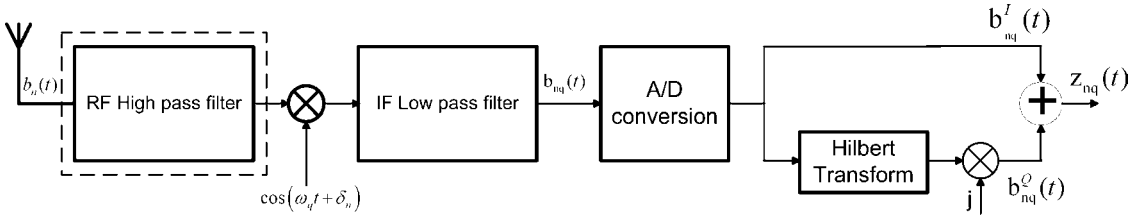

Fig. 2 *RF components and DSP for image suppression*

of achievable image suppression. The most significant of these is the variation of the RF-to-IF frequency response for two consecutive settings (scans) of the LO. To relate this to the image frequency suppression degradation, let the signal frequency w fall within the band $\omega_{01} < \omega < \omega_{02}$ and set the LO at w_{01}. Denote the resulting power at the IF filter output (possibly followed by amplifier) corresponding to the nth array element by $P^{(n)}(\omega - \omega_{01})$ and the IF power for the LO setting w_{02} (for the same input signal level) by $P^{(n)}(\omega_{02} - \omega)$. Then the image suppression is limited by

$$S^{(n)}(\omega)(\text{dB}) = 10\ \log_{10} \frac{P^{(n)}(\omega - \omega_{01})}{|P^{(n)}(\omega - \omega_{01}) - P^{(n)}(\omega_{02} - \omega)|} \tag{30}$$

For commercial off the shelf components (COT), the expected variation of $P^{(n)}(\omega - \omega_{01})/P^{(n)}(\omega_{02} - \omega)$ is not expected to be much better than about a 1 dB for which (30) gives only 6 dB. As shown in Section 4, using measured RF–to-IF transfer function data, digital compensators can be designed that can provide image suppression ratios in excess of 25 dB.

We comment here that once the sample data covariance matrix is estimated for the given sub-band according to the (29), any standard covariance-based DF algorithm can be applied to estimate the L_p signals incident in the pth sub-band. The eventual presence of the image frequency signals is treated on the same way as the presence of additive noise. Thus, if the singular value decomposition of the sample data covariance matrix is employed to estimate number of the incident signals L_p, all the signals with the corresponding singular values that are less than predefined threshold are discarded. In this particular case of the frequency-scanned DOA estimation system, the predefined threshold corresponds to an equivalent signal-to-noise ratio of 25 dB.

4 Experimental results

To validate the image suppression technique in the context of DOA estimation, a four-channel personal communications services frequency band (1850–1915 MHz) receiver with four A/D channels was implemented in hardware. The antenna array was emulated using RF phase shifters to yield the response of a 4-element linear array with identical radiation patterns to an incident plane wave. In a real physical antenna array, significant element pattern equalisation can be achieved either through a decoupling transform or with the aid of terminated dummy edge elements [7], thus permitting the use of root-based DOA algorithms. Detailed description of the hardware setup is provided in [8]. The four (nominally) equiphase RF signals are suitably time delayed by the four (continuously) adjustable spectrum RF phase shifters, thus emulating the outputs of a linear array with equalised element patterns. After downconversion, low-pass filtering and amplification stage, the four signals are fed to the A/D converter with an approximately -8 dB m signal power per channel. The signals are sampled at 25 MHz using two 2-channel 12-bit A/D cards with 10 effective bits, thus setting the upper limit on the SNR at almost 60 dB.

In order to compensate for the power variation of the IF signals as described by (30), a gain compensation function $C_n(\omega - \omega_{01})$ is used in the IF signal processing during the first scan such that

$$|C_n(\omega - \omega_{01})||H_n(\omega - \omega_{01})| = |H_n(\omega_{02} - \omega)| \tag{31}$$

where the transfer functions $H_n(\omega - \omega_{01})$ and $H_n(\omega_{02} - \omega)$ take account of the frequency dispersion of the low-pass filters, voltage amplifiers and mixers, as illustrated in Fig. 3. The compensator is determined from the measurement of

$$\Delta P_n(\omega) = 10\ \log \frac{P^{(n)}(\omega - \omega_{01})}{P^{(n)}(\omega_{02} - \omega)} \tag{32}$$

so that

$$|C_n(\omega - \omega_{01})| = 10^{\Delta P_n(\omega)/20} \tag{33}$$

Using (33), the compensator transfer function is computed for desired number of the frequency points in the baseband, that is, $0 < \omega - \omega_{01} < \omega_{02} - \omega_{01}$. In the implementation described herein, the IF band is $(\omega_{02} - \omega_{01})/2\pi = 5$ MHz. Once the desired frequency response of the gain compensator is determined, the impulse response is obtained from

$$c_n(t) = F^{-1}\{|C_n(\omega - \omega_{01})| \exp[-\text{j}(\omega - \omega_{01})\tau]\} \tag{34}$$

where in F^{-1} denotes inverse Fourier transform, $\tau = (M-1)/2$ and M is the order of the Finite Impulse Response (FIR) system used to implement gain compensator. The IF signal after downconversion with the LO frequency w_{01} is then given by

$$\text{Re}[\bar{z}_{n1}(t)] = c_n(t) * \text{Re}[z_{n1}(t)] \tag{35}$$

where * denotes temporal convolution. Equation (35) implies that the gain compensation is applied before transforming the received signal into the complex representation.

The LO frequencies used in the experiment were $f_{01} = 1910$ MHz and $f_{02} = 1915$ MHz. Frequency responses

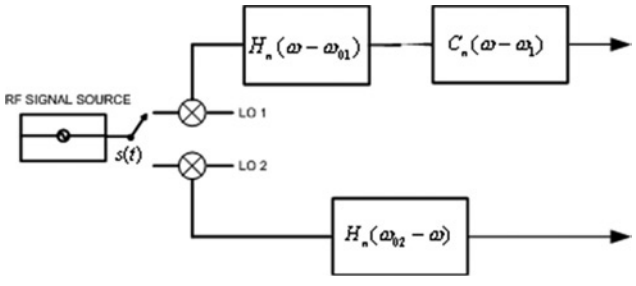

Fig. 3 *Relative positions of LO and bin centre frequencies for a scanned DOA system*

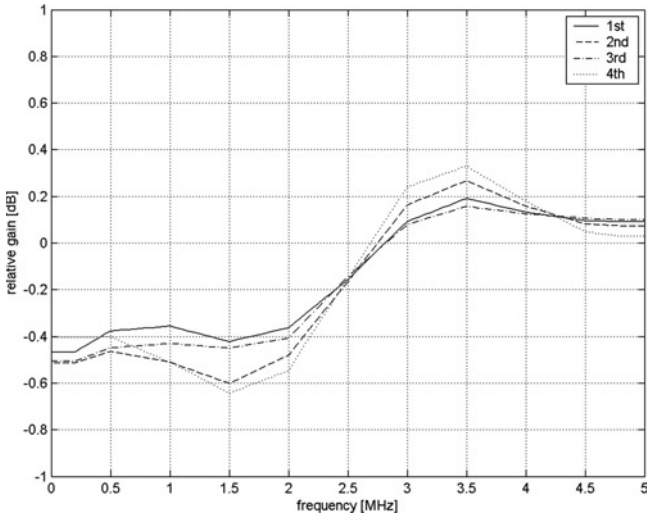

Fig. 4 *Magnitude response of the FIR gain equalizer in the IF band for each of the four channels*

Magnitude response refers to the gain difference between two adjacent RF sub-bands for the same IF
Line styles shown in the *upper right*
corner denote one of the four different channels

of the four IF channels were measured at 11 RF frequencies: 1910.2, 1910.5, 1911, 1911.5, 1912, 1912.5, 1913, 1913.5, 1914, 1914.5 and 1914.8 MHz. Fig. 4 shows magnitude frequency responses in dB scale of the FIR gain equalisers, [(33)], with the length of 512 taps. The equalisers are designed on the basis of measured gain differences by means of the frequency sampling method. The equaliser gain for each channel is denoted by the appropriate line style. Fig. 5 shows the image suppression factor (30) in dB without gain compensation. Except for a few cases, the image suppression ratio is seen to be less than 15 dB. Introducing gain compensation results in the plots shown in Fig. 6. Now the suppression ratio is always greater than 22 dB and in the majority of the cases greater than 30 dB that is better than can be achieved by the COT image rejection mixers [9]. The minimal rejection ratio of these COT image rejection mixers is 15–18 dB and typical 20–23 dB. Thus, we have demonstrated experimentally that software technique based on recursive subtraction of the

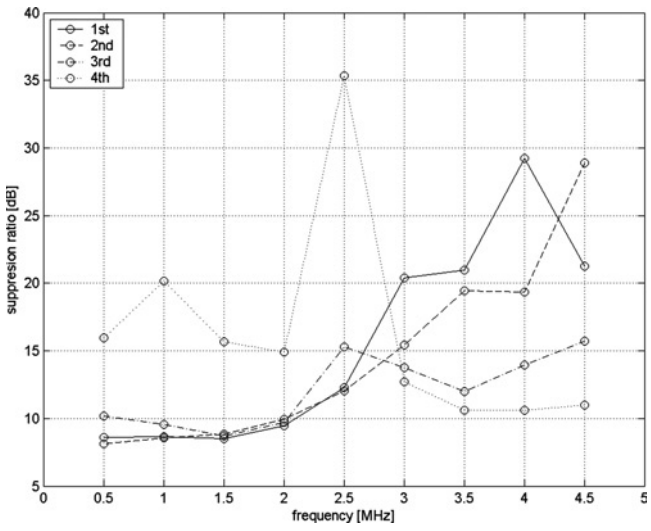

Fig. 5 *Image suppression ratio for each of the four channels without compensation of the gain difference between two adjacent RF sub-bands*

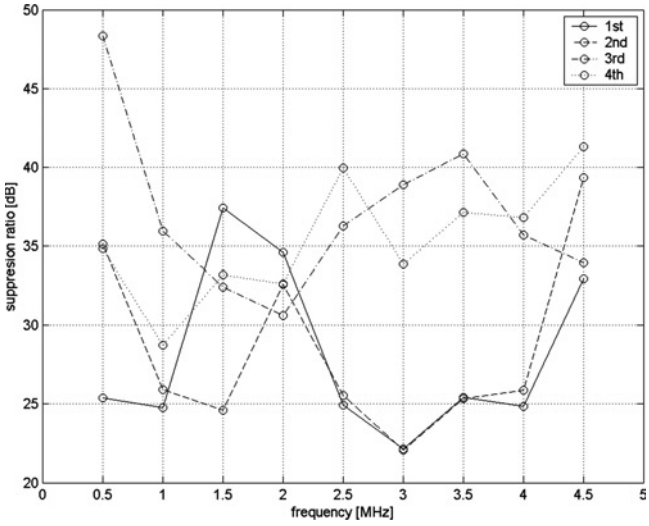

Fig. 6 *Image suppression ratio for each of the four channels after the gain difference between two adjacent RF sub-bands has been compensated*

sample data covariance matrix has in average 7–8 dB better image rejection performance.

Fig. 7 shows the DOA estimated by the MRP algorithm for a CW signal at 1913 MHz when the LO frequency is set to 1910 MHz (Fig. 8). The phase difference between

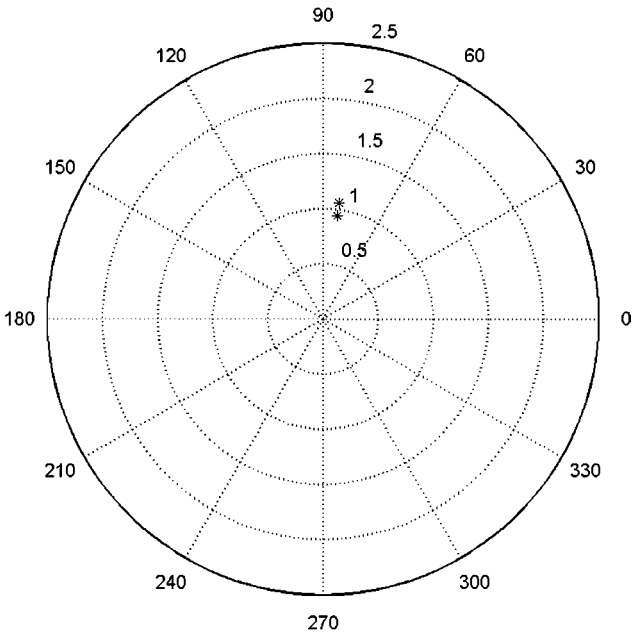

Fig. 7 *Polar plot of the estimated DOA with the LO set to 1910 MHz*

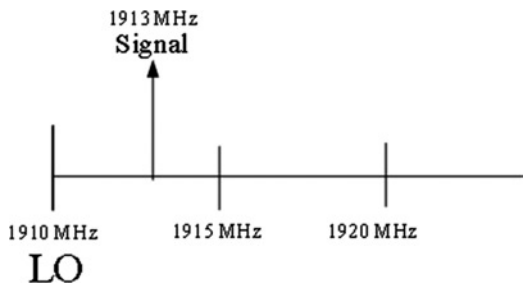

Fig. 8 *LO and signal spectrum positions during the scan of the first sub-band*

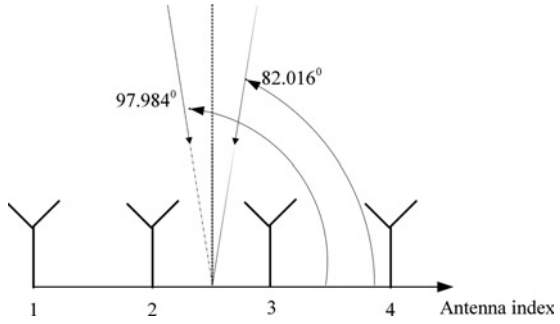

Fig. 9 *True and imaged DOA positions*

True DOA (82.016°) and imaged DOA (97.984°) positions obtained by scanning the first and second sub-band, respectively, when no image suppression is applied

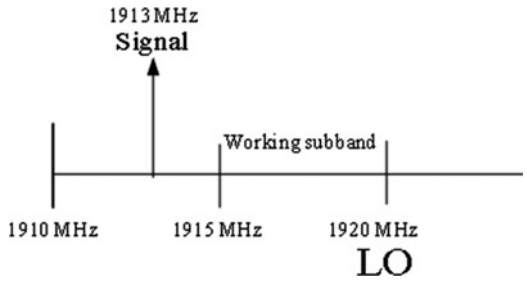

Fig. 10 *LO and signal spectrum positions during the scan of the second sub-band*

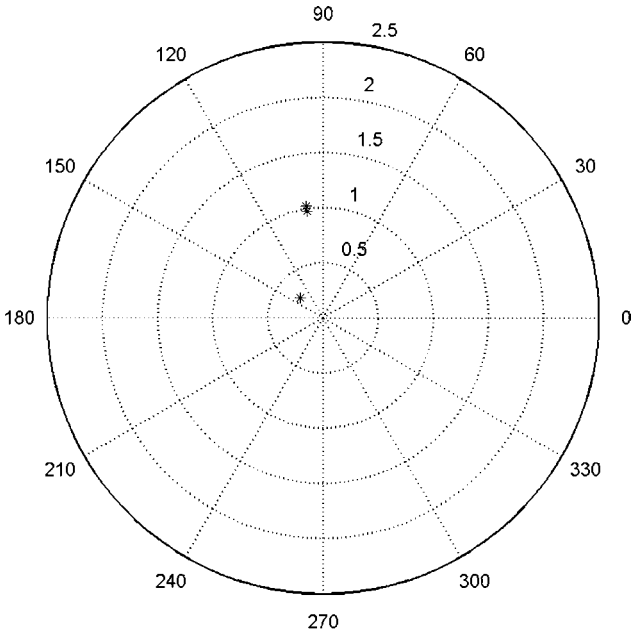

Fig. 11 *Polar plot of the estimated DOA with the LO set to 1915 MHz without gain compensation*

the adjacent phase shifters channels was set to 25° which for inter-element spacing of $l/2$ corresponds to an angle of incidence of 82.0164° with respect to the array axis as indicated in Fig. 9. The DOA actually estimated by the MRP algorithm was 82.0083°, giving an error of 0.008°. Next the LO frequency was moved to 1915 MHz for DOA estimation of signals falling in the 1915–1920 MHz sub-band (Fig. 10). Because this sub-band is empty, the only signal that will be downconverted to baseband is the one in the first sub-band, that is, the image frequency. Using the covariance subtraction technique without gain compensation yields a DOA estimate of the image at 98.5° (theoretical value 97.9835°, see Fig. 9) as indicated in the polar plot in Fig. 11. The reason that the image is not suppressed can be seen from Fig. 5 where for an IF frequency of 2 MHz the image suppression ratio is only about 10 dB. On the other hand, no image signal was detected with gain compensation, a credible result in view of the greater than 30 dB image suppression ratio that can be read off the graph in Fig. 6 at 2 MHz. This example indicates what performance can be obtained by the COT image rejection mixers [9], in the worst-case scenario with the image rejection of 15 dB only. Thus, this result demonstrates that in relation to the frequency-scanned DOA estimation systems based on COT image suppression frequency mixers, presented procedure poses improved image frequency rejection using at the same time significantly cheaper single-channel mixers.

5 Conclusion

A DOA estimation procedure was described and validated experimentally that employs a novel signal processing scheme for image suppression requiring only single-channel downconversion per array element. The advantages of this approach are that only one A/D converter per array element is required and that the hardware implementation is potentially less expensive than the use of image rejection mixers. In particular, we have demonstrated experimentally that image rejection performance of COT versions of image rejection mixers is on average 7–8 dB poorer compared to what can be achieved with the proposed technique. Thus, compared with frequency-scanned DOA estimation systems employing COT image frequency mixers, our approach provides improved image frequency rejection performance when at the same time using significantly cheaper single-channel mixers. This should be of the practical importance in the design of frequency-scanned DOA estimation systems, especially when a large number of array elements is needed.

6 References

1 Schmidt, R.O.: 'A signal subspace approach to multiple emitter location and spectral estimation', PhD dissertation, Stanford University, 1981
2 Rao, B.D., and Hari, K.V.S.: 'Performance analysis of root – MUSIC', *IEEE Trans. Acoust. Speech Signal Process.*, 1989, **34**, (12), pp. 1939–1949
3 Barabell, A.J.: 'Improving the resolution performance of eigenstructure-based direction-finding algorithms'. Proc. ICASSP, Boston, MA, 1983, pp. 336–339
4 Gönen, E., and Mendel, J.: 'Subspace-based direction finding methods'' in 'The digital signal processing handbook' (CRC Press, 1998), Ch. 62, pp. 62-1–62-23
5 Wasylkiwskyj, W., and Kahn, W.K.: 'Theory of mutual coupling among minimum scattering antennas', *IEEE Trans. Antennas Propag.*, 1970, **18**, (2), pp. 204–216
6 Allen, O., and Wasylkiwskyj, W.: 'Antenna pattern synthesis in operational environments with electromagnetic compatibility constraints', *IEEE Trans. Electromagn. Compat.*, 2004, **46**, (4), pp. 668–674
7 Lundgren, S.: 'A study of mutual coupling effects on the direction finding performance of ESPRIT with a linear microstrip patch array using the method of moments'. IEEE AP-S Symp., Baltimore, July 1996, pp. 1372–1375
8 Wasylkiwskyj, W., Kopriva, I., Doroslovački, M., and Zaghloul, A.I.: 'A new root-based direction finding algorithm', *Radio Sci.,* in press
9 http://miteq.com/micro/mixers/special/sec21.htm